High Performance Temperature Difference Triboelectric Nanogenerator

Bolang Cheng
Lanzhou University
Qi Xu
Xidian University https://orcid.org/0000-0003-0546-5360
Yaqin Ding
Lanzhou University
Suo Bai
Lanzhou University
Xiaofeng Jia
Lanzhou University
Yangdianchen Yu
Boston University
Yong Qin (qinyong@lzu.edu.cn)
Lanzhou University https://orcid.org/0000-0002-6713-480X

Article

Keywords: triboelectric nanogenerator, high temperature, charge density, performance

Posted Date: September 9th, 2020

DOI: https://doi.org/10.21203/rs.3.rs-65933/v1

Version of Record: A version of this preprint was published at Nature Communications on August 6th, 2021. See the published version at https://doi.org/10.1038/s41467-021-25043-2.

High Performance Temperature Difference Triboelectric Nanogenerator

Bolang Cheng[1,†], Qi Xu[2,†], Yaqin Ding[1,†], Suo Bai[1], Xiaofeng Jia[1], Yangdianchen Yu[1,3], Yong Qin[1,*]

[1] Institute of Nanoscience and Nanotechnology, Lanzhou University, Lanzhou 730000, China.

[2] School of Advanced Materials and Nanotechnology, Xidian University, Xi'an 710071, China.

[3] Department of Material Science and Engineering, College of Engineering, Boston University, Boston, MA, 02215, U. S.

[†] Authors with equal contribution

*Corresponding author. E-mail: qinyong@lzu.edu.cn

Abstract: Usually, high temperature decreases the output performance of triboelectric nanogenerator (TENG) because of the dissipation of triboelectric charges through the thermionic emission. It would be highly valuable if the high temperature can be used to enhance the output performance of TENG. In this paper, through a simulation combining the electron-cloud-potential-well model for triboelectrification and the thermionic-emission model, we find that there exists an optimum temperature difference ΔT between friction layers under which the output of TENG is maximum. Based on this, a type of contact-separation temperature difference TENG with controllable friction layer temperature (TDNG) is designed and fabricated to enhance the electrical output performance in temperature difference environment. As the temperature difference ΔT increasing from 0 K to 145 K, the output voltage, current, the surface charge density and output power are increased 2.7, 2.2, 3.0 and 2.9 times, respectively (from 315 V, 9.1 μA, 47 nC/m^2, 69 μW to 858 V, 20 μA, 0.14 μC/m^2,

206.7 μW). Then with the continuous increase of ΔT to 219 K, the surface charge density and output performance gradually decrease. At the optimal temperature difference (145 K), the biggest output current density (396 μA/cm^2) has been obtained, which is 13% larger than the reported record value (350 μA/cm^2).

1. Introduction

Based on the coupling effect of the contact electrification and electrostatic induction, triboelectric nanogenerators (TENG) have been successfully developed for mechanical energy harvesting and self-powered active sensors.[1-3] To obtain higher electrical output performance, lots of works have been done including material selection,[4-6] structural optimization,[7-10] artificial prior-charge injection,[11, 12] coupling surface polarization and hysteretic dielectric polarization in vacuum.[13] The relationship between output performance and materials, structure, friction areas, surface charge density, external forces, working frequency, etc. has also been studied.[14-16] Recently, current densities of 25.2 μA/cm^2 and 28.8 μA/cm^2 in atmosphere have been obtained by a pumping TENG[17] and a self-charge excitation TENG system[18], respectively. The output can be improved to 57 μA/cm^2 by operating TENG in vacuum environment[13] and to 90 μA/cm^2 by artificial prior-charge injection [11]. With an electric double-layer structure designed in TENG, 305 μA/cm^2 output can be obtained.[10] Moreover, by using materials easier to gain/loss charges and fabricating micro/nanostructure to enlarge friction areas at the same time, the largest current density has been improved to 350 μA/cm^2.[19]

Apart from room temperature, TENGs need to work at high temperature in some particular applications such as harvesting the vibration energy of automobile engine. But when the whole working temperature of TENG is higher than 260 K, its output decreases significantly,[20, 21] as the temperature of friction material will affect the storage and dissipation of electrons during triboelectrification.[22, 23] In recent years, the electron thermionic emission in TENG has been studied[20, 22-24], which is used to explain the influence of temperature on the electrical output performance of TENG. Comparing with the whole and homogeneous temperature of TENG, the temperature

difference between two friction layers is another important and more complex influence factor. Later, on the premise of fixing the temperature of the cooler end-tip, through increasing the temperature of the dielectric sample's surface to strictly control the temperature difference between them, the study of electrons transfer processes in nanoscale reveals that the temperature difference will facilitate electrons transferring from hotter materials to cooler materials, and the charge density can be improved notably in a particular temperature difference range.[24] Although this work is done in nanoscale by using an atomic force microscope (AFM) tip, it gives a possibility in principle that the temperature difference between two friction layers can be utilized to enhance the output of TENG through rational design. In addition, temperature difference widely exists in some special conditions, such as the surface of engine and the exhaust pipe of automobile. If both temperature difference energy and vibration energy of automobile can be effectively converted into electricity, it is very beneficial for the comprehensive monitoring of automobile and car networking, et al. For other conditions such as the surface of airplane's engine, the temperature difference and vibration have the same potential application value for the real-time monitoring of airplane. Besides the thermoelectric technology, pyroelectric technology, and their combination with mechanical energy, if the temperature difference can be used to greatly increase the energy conversion efficiency of TENG, it will provide a new way to high-efficiently harvest and utilize the temperature difference and vibration energy. Generally, in practical conditions, the temperature of the cooler friction layer will also rise in practical applications due to the heat exchange in contact-separation processes and air heat transfer, which will decrease the TENG's output performance. So, it is very important to enhance the output of TENG through utilizing the high temperature and temperature difference in practical application conditions, but it is still a great challenge by now.

In this study, the high temperature and temperature difference in TENG are studied theoretically, and the optimum temperature difference between friction layers for improving TENG's output is given. A new type of temperature difference TENG with controllable friction layer temperature (TDNG) is successfully designed and

fabricated to enhance the electrical output performance of TENG to a new record. As the temperature difference between hotter and cooler friction layers (ΔT) increasing from 0 K to 219 K, the electrical output performances of TDNG increase at first and then decrease. Under the optimal ΔT (~145 K), the open-circuit voltage of 858 V, short-circuit current of 20 μA, surface charge density of 0.14 μC/m^2 and output power of 206.7 μW are 2.7, 2.2, 3.0 and 4.9 times the output values when ΔT equals to 0 K, respectively. Furthermore, by optimizing the friction materials of the TDNG, the current density is enhanced to 396 μA/cm^2 which is 13% larger than the record value (350 μA/cm^2).

2. Results and Discussion

2.1 Numerically analysis of the influence of ΔT on electrical performance of TENG

Take the heat exchanges between hotter and cooler friction layers into account, the temperature of the cooler friction layer will continuously rise through air and contacting heat transfer, and the accumulated charges of cooler friction layer will gradually escape to air as well as the hotter friction layer by thermally stimulated discharging. Here, an electron-cloud-potential-well model shown in **Figure 1**a is used to explain the electrons transfer process for contact electrification between hotter and cooler friction layers when temperature difference exists between the hotter and cooler frication layers. As the left part of **Figure 1**a shows, the hotter friction layer's electron energy levels will increase ($\approx k\Delta T$) due to the raised temperature. On the one hand, during friction, more electrons will hop from the hotter friction layer to cooler friction layer (middle part of **Figure 1**a) to enhance the charge density. On the other hand, the increased temperature of cooler friction layer will discharge the electrons accumulated in cooler friction layer (electrons are easier to escape out of the potential well, and get back to the hotter friction layer in contact processes or spill into air, as the right part of **Figure 1**a shows), and lead to reduce charge density and output performance of TENG. Therefore, there should exist an optimal temperature difference that can boost the output performance of TENG.

Numerical simulations are carried out using COMSOL to verify the above model. During the simulation, charge transferred from hotter friction layer to cooler friction layer as well as the charge dissipation from the cooler friction layer due to thermionic emission [23, 25] are considered simultaneously. In the first stage, as the inset in the right upper corner of **Figure 1**b shows, the temperature of cooler friction layer increases approximate linearly with the temperature of hotter friction layer. With the temperature of hotter friction layer further increases, the temperature of the cooler friction layer increases slowly. According to the linear relationship between charge density and temperature of hotter friction materials (Equation (1)), and the modified thermionic emission model (Equation (2)):

$$\sigma = -C_1 T_h + C_2 \tag{1}$$

$$\sigma_{tc} = e^{-SAT}\sigma_{tc0} \tag{2}$$

where σ is the surface charge density when the temperature of the cooler friction layer keep fixed, T_h is the temperature of hotter friction layer, C_1 and C_2 are the material-related correction factors, σ_{tc} is the short-circuit transfer charge density, and σ_{tc0} is the initial value of σ_{tc}(equal the value of σ), $S = \frac{\lambda_1 A_0}{k} T e^{\frac{qv}{kT}}$, where λ_1 is the material-specific correction factor, A_0 is Richardson constant of a free electron, T is the temperature of friction material, k is Boltzmann constant, the relationship between surface charge density of cooler friction layer (assume that the surface charge density is equal to the transferred charge density) and ΔT (ΔT=T_h-T_c, where T_h is the temperature of the hotter friction and T_c is the temperature of the cooler friction layer) is calculated (**Figure 1**b). Different from what in an ideal nanoscale situation (linearly increased transferred charges density with ΔT),[24] the transferred charges density and surface potential (**Figure 1**c) of TENG will firstly increase and then decrease when ΔT increases to a certain level (above 220 K in simulation). Accordingly, if TENG works with a suitable temperature difference between friction layers, it can output a maximum electrical performance due to the enhanced surface charge density and higher transferred charges density.

2.2 Fabrication and electrical output performance of TDNG

Based on the theoretical analysis mentioned above, a TDNG includes a hotter part and a cooler part with a separation of air gap (as shown in **Figure 2**a) is designed and fabricated. Both the hotter part and cooler part include 3 layers: friction layer, electrode film, and temperature controllable heat/cool layer. Compared with previous TENGs, such design can control the temperature of friction layers effectively, and it is convenient to study the influence of temperature difference on the output of TDNG. The friction layer in the hotter part and cooler part are the chemical reactive etched 20-μm-thick aluminum (Al) foil and directly reactive ion etched (RIE) 100-μm-thick Kapton film, respectively. The nanostructures fabricated on them can enhance the contact area during triboelectrification and improve TDNG's electrical output performance, as illustrated in the insets of **Figure 2**a.

To study the relationship between the output performance of TDNG and ΔT, a linear motor (K15-W/C-2, LinMot) is used to drive the TDNG. The open-circuit voltage and short-circuit current at different ΔT are shown in **Figure 2**b. In accordance with the simulation, with the ΔT increasing from 0 K to 219 K, the output voltage and current of TDNG increase at first and then decrease. The largest output voltage and current can reach to 858 V and 20 μA when ΔT equals to 145 K, as the temperature of cooler friction layer (T_c) keeps 299 K. Under this optimal ΔT, the output voltage and current are 2.7 and 2.2 times the values when ΔT equals to 0 K (314.5 V, 8.98 μA).

To further study the effect of ΔT on TDNG's performance, the transferred short-circuit charge quantities per cycle (CQC) of TDNG under different ΔT have been calculated and illustrated in **Figure 3**a. Under the optimal ΔT (145 K), the CQC is 147 nC (corresponding a surface charge density of 0.14 μC/m^2), which is 3 times the CQC when ΔT equals to 0 K at room temperature. In addition, to give a clearer illustration of the importance of temperature difference on TDNG, a thermally stimulated discharge (TSD) current is carried out to evaluate the number of accumulated charges on Kapton (the accumulated charges in friction layer is positively related the surface charge

density). As the schematic diagram of TSD testing device (Supplementary Figure S1) illustrates, when a charged Kapton film is heated by a hot system (the temperature rising curves of heating system in TSD testing is shown in Supplementary Figure S2), the accumulated charges in Kapton will gradually escape from the potential well and a current peak is formed. **Figure 3**b illustrates the TSD curves of Kapton after friction at different ΔT. When ΔT increases from 0 K to 192 K, the time integral of current increases from 0 K to 155 K, and decreases when ΔT is above 155 K, which means the accumulated charges in Kapton reach maximum under 155 K. Moreover, the surface potentials of Kapton can intuitively reflect the advantages of ΔT in triboelectrification. As shown in **Figure 3**c, the largest surface potential of -112 V has been obtained with ΔT equals 145 K and the same trend as mentioned above has been observed. With the certificate of transferred short-circuit current charges, TSD current curves, and surface potential of Kapton, there exists an optimal ΔT that can effectively boost the output of TDNG through improving the accumulated friction charges in cooler friction layer.

2.3 Output performance enhancement of TDNG through material's optimization and its applications

In addition, the advantages of temperature difference in TENG is illustrated by the dependence of TDNG's output performance on external resistance. As shown in **Figure 4**a, the voltage and current show opposite trend with the increased resistance of external load, and all of them at optimal ΔT are higher than that without ΔT. The output power of the TDNG reaches maximum when the external resistance is 3 MΩ. Under the optimal ΔT, the maximum output power increases from 42.2 μW to 206.7 μW (**Figure 4**b). Therefore, through combining temperature difference and triboelectrification in TDNG, the power supply capacity of TDNG can be improved effectively (4.9 times compared with that without temperature difference).

In order to investigate the effectiveness and versatility of the temperature difference effect in TENG and further enhancing output performance of TENG, TDNGs with different friction layers including Al-Kapton, polyamide 6 (PA6)-Kapton, copper (Cu)-Kapton, iron (Fe)-Kapton, and Al-polytetrafluoroethylene (PTFE)

(nanostructure of PTFE and PA6 are shown in Supplementary Figure S3) have been studied. As shown in **Figure 4**c-d, the output of all these TDNGs can be improved when ΔT is constructed between two friction layers. Corresponding to Al-Kapton, PA6-Kapton, Cu-Kapton, Fe-Kapton, and Al-PTFE TDNGs, the open-circuit voltages have enhanced 2.7, 3.2, 3.0, 3.9, 2.7 times at optimal ΔT, and the short-circuit currents have enhanced 2.2, 2.0, 2.6, 10, 1.7 times at optimal ΔT (**Figure 4**d and **Table 1**). In this way, the output performance of TDNG can be enhanced effectively by optimizing the friction materials of the TDNG. Besides, the optimal ΔT is related to the materials of the cooler friction layer (as shown in **Table 1)**, where the optimal ΔT is about 144 K when cooler friction layer is Kapton. However, when PTFE is used as the cooler friction layer, the optimal ΔT is just 90 K. Furthermore, with the help of materials optimizing, the largest open-circuit voltage can reach to 1.5 kV **(Figure 4**e), and a largest short-circuit current density can reach to 396 μA/cm^2 **(Figure 4**f) for Al-PTFE TDNG, which is 13% larger than the record value (350 μA/cm^2).[19] In this way, the effectiveness and universalism of the temperature difference effect in TENG has been investigated, and the highest output current density in contact-separation TENG is achieved simply without complex structure optimization, material preparation or excessively artificial treatment.

Compared with other TENGs, TDNG can be used for harvesting mechanical energy on high-temperature objects more efficiently. Here, a wind-driven TDNG is designed and put on the surface of hot objects to simulate a practical application on high-temperature objects like a car hood, hot road and roof. As the upper part of **Figure 5**a shows, an etched and fixed Al plate is flattened against hot plate serving as a hotter part of wind-driven TDNG, and an etched Kapton flag is hanging in the air serving a cooler part. Under continuous wind, the bottom part of **Figure 5**a illustrates the short-circuit current of the wind-driven TDNG in different ΔT under wind speed of 15 m/s. The maximum current can reach to 143 μA when ΔT equals to 128 K. Via a rectifier, a 1 μF capacitor can be charged from 0 V to 7 V within 15 s (orange line, ΔT equals to 128 K), compared with ΔT equals to 0 K (black line) and 79 K (pink line), the

capacitor has the fastest charging rate, and a highest saturation voltage (**Figure 5**b). With the help of a filter circuit (Supplementary Figure S4), blue LEDs can be lightened continuously, where the brightness and lighted number of LEDs can be used as an indicator for temperature monitoring (**Figure 5**c). Additionally, after a short-time storage, a temperature-humidity sensor can be powered by the wind-driven TDNG under conditions of ΔT equals to 102 K with a wind speed of 10 m/s (**Figure 5**d).

3. Conclusion

In summary, the effect of temperature difference on TENG performance has been investigated through a simulation combining electron-cloud-potential-well model for triboelectrification and the thermionic-emission model, and a novel type of TENG with controllable friction layer temperature has been designed and fabricated to boost the electrical output performance. With the increasing of temperature difference, the output of TDNG increases at first and then decreases due to a tradeoff between electrons transfer from hotter friction layer to cooler friction layer and thermionic-emission induced electrons discharge from cooler friction layer. Under the optimal ΔT, the open-circuit voltage, short-circuit current, surface charge density and output power of the Al-Kapton TDNG increase 2.7, 2.2, 3.0 and 4.9 times compared to the case when ΔT equals to 0 K. The construction of the frication layer temperature difference can be extended to other TENGs to also boost their outputs. Changing the friction materials from Al-Kapton to Al-PTFE, the current density of TDNG is further enhanced to 396 $\mu A/cm^2$, which is 1.13 times the record value (350 $\mu A/cm^2$). Finally, a wind-driven TDNG is demonstrated to power a temperature-humidity sensor to show its promising application in an environment with temperature difference.

Experimental section

Materials and chemicals. A 20-μm-thick Al, 20-μm-thick Cu film, and 20-μm-thick Fe plate are used for fabricating the hotter part of TDNG; a 100-μm-thick Kapton and a 50-μm-thick PTFE are used for fabricating the cooler part of TDNG. PA6 (Sinopharm Chemical Reagent Co., Ltd) is used for the fabrication of the electron

losing friction material of the hotter part of Nylon-Kapton TDNG. NaOH (>96%, Tianjin Baishi Chemical Co., Ltd) is used for etching Al film. Ethanol (>99%, Lian longbohua (Tianjin) Pharmaceutical Chemistry Co., Ltd) and deionized (DI) water are used for cleaning materials and devices.

Fabrication of Al-Kapton TDNG. Firstly, a piece of Kapton film with a thickness of 100 μm is cut into 5 cm × 5 cm, and ultrasonically cleaned with acetone, ethanol and deionized water for 15 minutes in sequence. After being dried by nitrogen, Cr/Ag electrode with a size of 4.8 cm × 4.8 cm is sputtered on the middle the Kapton film on one side. The other side of Kapton film is etched by RIE for 1 h with 3 sccm Ar and 7 sccm CF_4, 250 W input power. Secondly, a piece of cleaning Al film with a thickness of 20 μm are cut into 5 cm × 5 cm and then immersed in 0.5 mol/L NaOH solution for 2 minutes. After being washed by deionized water, the etched Al film is dried in a 333 K oven. Finally, placing the Al film on a hot layer to form a hotter part and Kapton film on a cool layer to form a cooler part. The hotter part and cooler part compose the TDNG and air gap between the hotter part and cooler part is 5 cm.

Measurement and Characterization. Morphology of the samples were characterized by emission scanning electron microscopy Apreo S. The output current signals of TDNG are measured by a low-noise current preamplifier Stanford Research SR570. For the measurements of the wind-driven TDNG, a commercial air gun is used and a hand-held anemometer is used for measuring wind speed.

Data availability

All data needed to evaluate the conclusions in the paper are present in the paper and/or the Supplementary Information. Additional data related to this paper may be requested from the authors.

Reference

1. Luo, J. et al. Flexible and durable wood-based triboelectric nanogenerators for self-powered sensing in athletic big data analytics. *Nature Communication* **10**, 5147 (2019).
2. Luo, J. & Wang, Z.L. Recent advances in triboelectric nanogenerator based self-charging power systems. *Energy Storage Materials* **23**, 617-628 (2019).
3. Chen, J. et al. Micro-cable structured textile for simultaneously harvesting solar and mechanical energy. *Nature Energy* **1**, 16138 (2016).
4. Docampo, P. et al. Lessons learned: from dye-sensitized solar cells to all-solid-state hybrid devices. *Advanced Materials* **26**, 4013-4030 (2014).
5. Cui, N. et al. Dynamic Behavior of the Triboelectric Charges and Structural Optimization of the Friction Layer for a Triboelectric Nanogenerator. *ACS Nano* **10**, 6131-6138 (2016).
6. Long, M. et al. Broadband Photovoltaic Detectors Based on an Atomically Thin Heterostructure. *Nano Letters* **16**, 2254-2259 (2016).
7. Wang, S., Lin, L. & Wang, Z.L. Nanoscale triboelectric-effect-enabled energy conversion for sustainably powering portable electronics. *Nano Letters* **12**, 6339-6346 (2012).
8. Zhu, G. et al. Toward large-scale energy harvesting by a nanoparticle-enhanced triboelectric nanogenerator. *Nano Letters* **13**, 847-853 (2013).
9. Cheng, G., Lin, Z.-H., Du, Z. & Wang, Z.L. Increase Output Energy and Operation Frequency of a Triboelectric Nanogenerator by Two Grounded Electrodes Approach. *Advanced Functional Materials* **24**, 2892-2898 (2014).
10. Chun, J. et al. Boosted output performance of triboelectric nanogenerator via electric double layer effect. *Nature Communication* **7**, 12985 (2016).
11. Wang, S. et al. Maximum surface charge density for triboelectric nanogenerators achieved by ionized-air injection: methodology and theoretical understanding. *Advanced Materials* **26**, 6720-6728 (2014).
12. Wang, Z., Cheng, L., Zheng, Y., Qin, Y. & Wang, Z.L. Enhancing the performance of triboelectric nanogenerator through prior-charge injection and its application on selfpowered anticorrosion. *Nano Energy* **10**, 37-43 (2014).
13. Wang, J. et al. Achieving ultrahigh triboelectric charge density for efficient energy harvesting. *Nature Communication* **8**, 88 (2017).

14. Wang, Z.L. Triboelectric nanogenerators as new energy technology and self-powered sensors - principles, problems and perspectives. *Faraday discussions* **176**, 447-458 (2014).

15. Chen, J. & Wang, Z.L. Reviving Vibration Energy Harvesting and Self-Powered Sensing by a Triboelectric Nanogenerator. *Joule* **1**, 480-521 (2017).

16. Fan, F.R. et al. Transparent triboelectric nanogenerators and self-powered pressure sensors based on micropatterned plastic films. *Nano Letters* **12**, 3109-3114 (2012).

17. Xu, L., Bu, T.Z., Yang, X.D., Zhang, C. & Wang, Z.L. Ultrahigh charge density realized by charge pumping at ambient conditions for triboelectric nanogenerators. *Nano Energy* **49**, 625-633 (2018).

18. Liu, W. et al. Integrated charge excitation triboelectric nanogenerator. *Nature Communication* **10**, 1426 (2019).

19. Kim, M. et al. Remarkable Output Power Density Enhancement of Triboelectric Nanogenerators via Polarized Ferroelectric Polymers and Bulk MoS2 Composites. *ACS Nano* **13**, 4640-4646 (2019).

20. Lu, C.X. et al. Temperature Effect on Performance of Triboelectric Nanogenerator. *Advanced Engineering Materials* **19**, 1700275 (2017).

21. Wen, X., Su, Y., Yang, Y., Zhang, H. & Wang, Z.L. Applicability of triboelectric generator over a wide range of temperature. *Nano Energy* **4**, 150-156 (2014).

22. Xu, C. et al. Raising the Working Temperature of a Triboelectric Nanogenerator by Quenching Down Electron Thermionic Emission in Contact-Electrification. *Advanced materials* **30**, 1803968 (2018).

23. Xu, C. et al. On the Electron-Transfer Mechanism in the Contact-Electrification Effect. *Advanced materials* **30**, 1706790 (2018).

24. Lin, S. et al. Electron Transfer in Nanoscale Contact Electrification: Effect of Temperature in the Metal-Dielectric Case. *Advanced materials* **31**, 1808197 (2019).

25. Lin, S., Xu, L., Tang, W., Chen, X. & Wang, Z.L. Electron transfer in nano-scale contact electrification: Atmosphere effect on the surface states of dielectrics. *Nano Energy* **65**, 103956 (2019).

Acknowledgments

This research was supported by the support from Joint fund of Equipment pre-Research and Ministry of Education (NO. 6141A02022518), the National Program for Support of Top-notch Young Professionals, the Fundamental Research Funds for the Central Universities (No. lzujbky-2018-ot04), NSFC (NO. 81702095, 81801847).

Author contributions

B.C., Y.D. and Q.X. contributed equally to this work. Y.Q., B.C. and Y.D designed the TDNG, B.C., Q.X. and S.B. fabricated and measured the device, X.J. and Q.X. conducted the simulation via COMSOL, B.C., Y.D., S.B., and Y.Y. analyzed the experimental data, plotted the figures and prepared the manuscript, and all authors reviewed and commented on the manuscript.

Competing interests

The authors declare no conflict of interest.

Additional information

Supplementary Information is available for this paper.

Correspondence and requests for materials should be addressed to Y.Q.

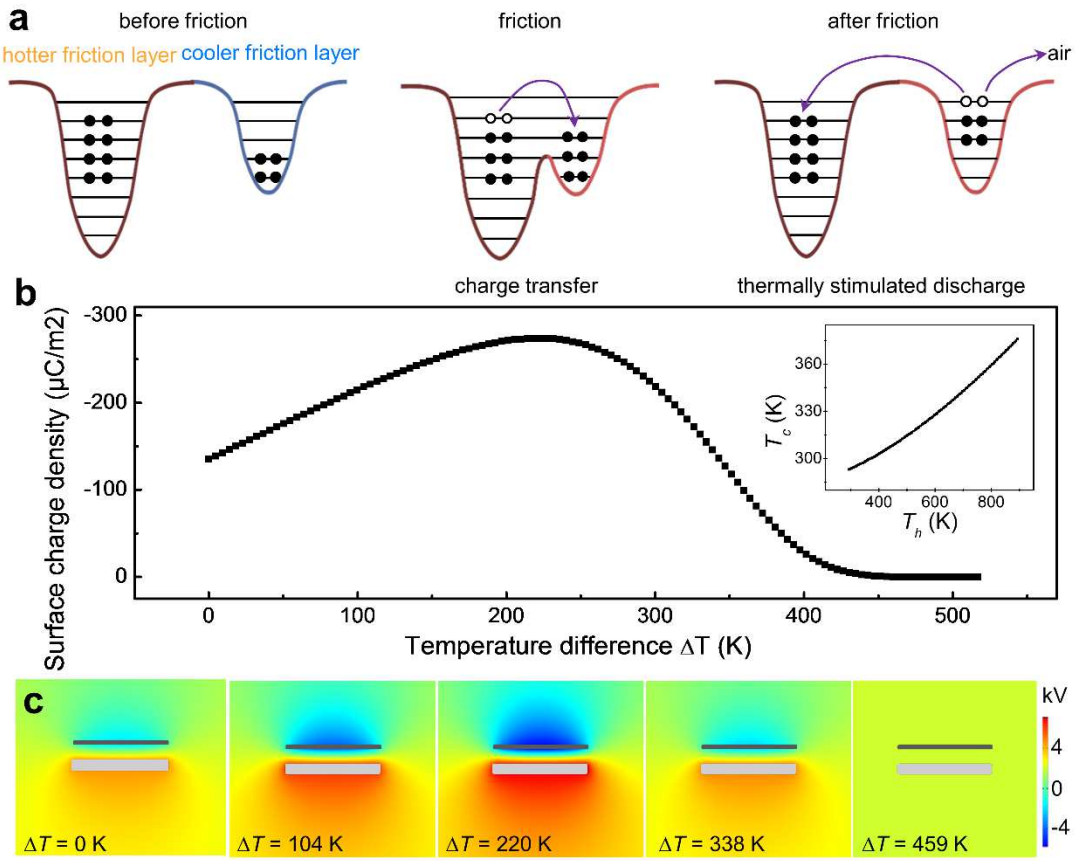

Figure 1. The influence of temperature difference between different friction layers on TENG's performance. (**a**) Effect of ΔT on charge transfer and dissipation. (**b**) Numerical simulations of the relationship between ΔT and the short-circuit transfer charge density. The right upper is the relationship between the temperature of the hotter part and the cooler part. (**c**) The potential distribution of TENG under different ΔT.

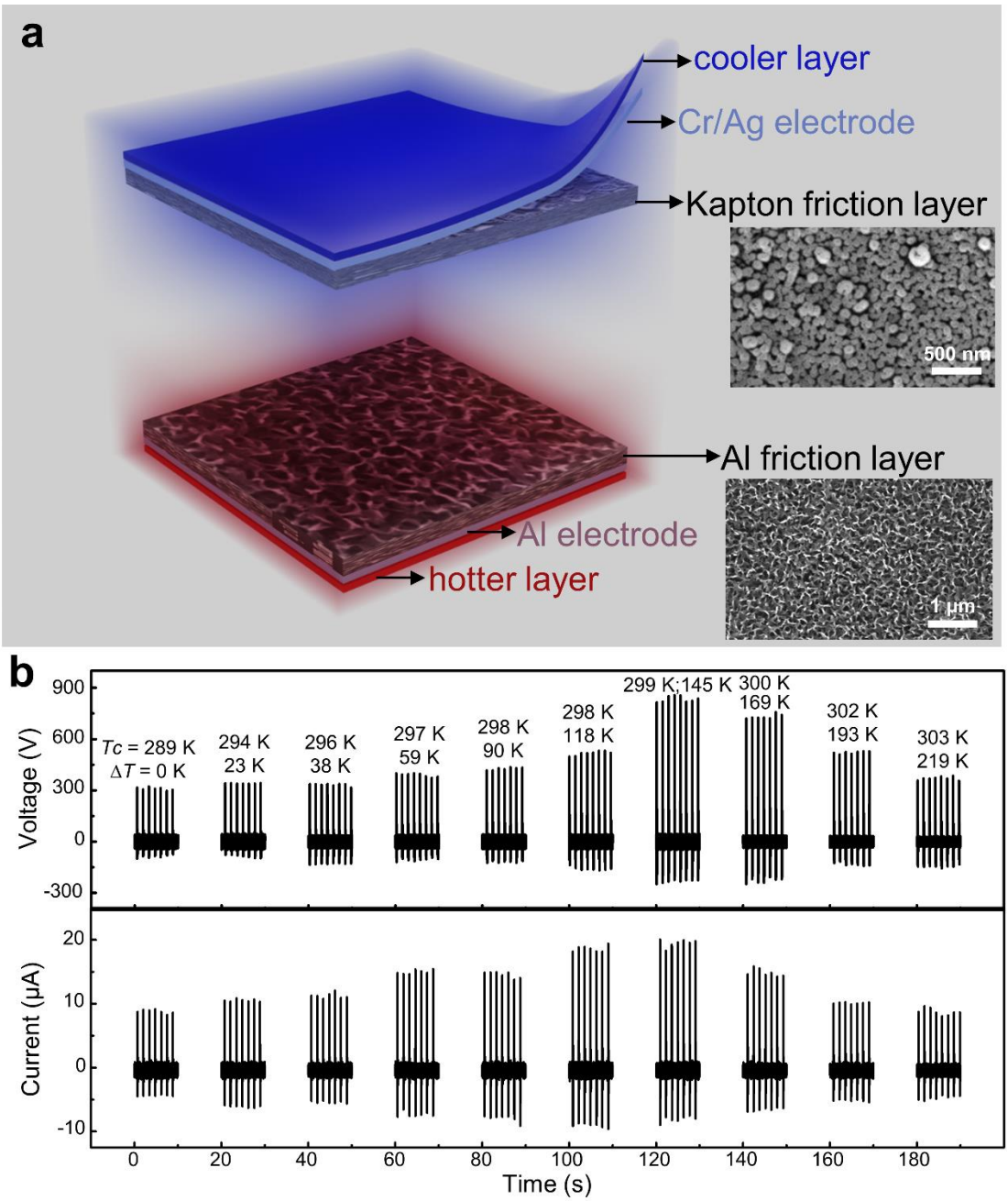

Figure 2. Design and output performance of TDNG. (**a**) Schematic diagram of TDNG. Insert are SEM images of nanostructures on Kapton and Al. (**b**) The open-circuit voltage and short-circuit current of TDNG under different ΔT.

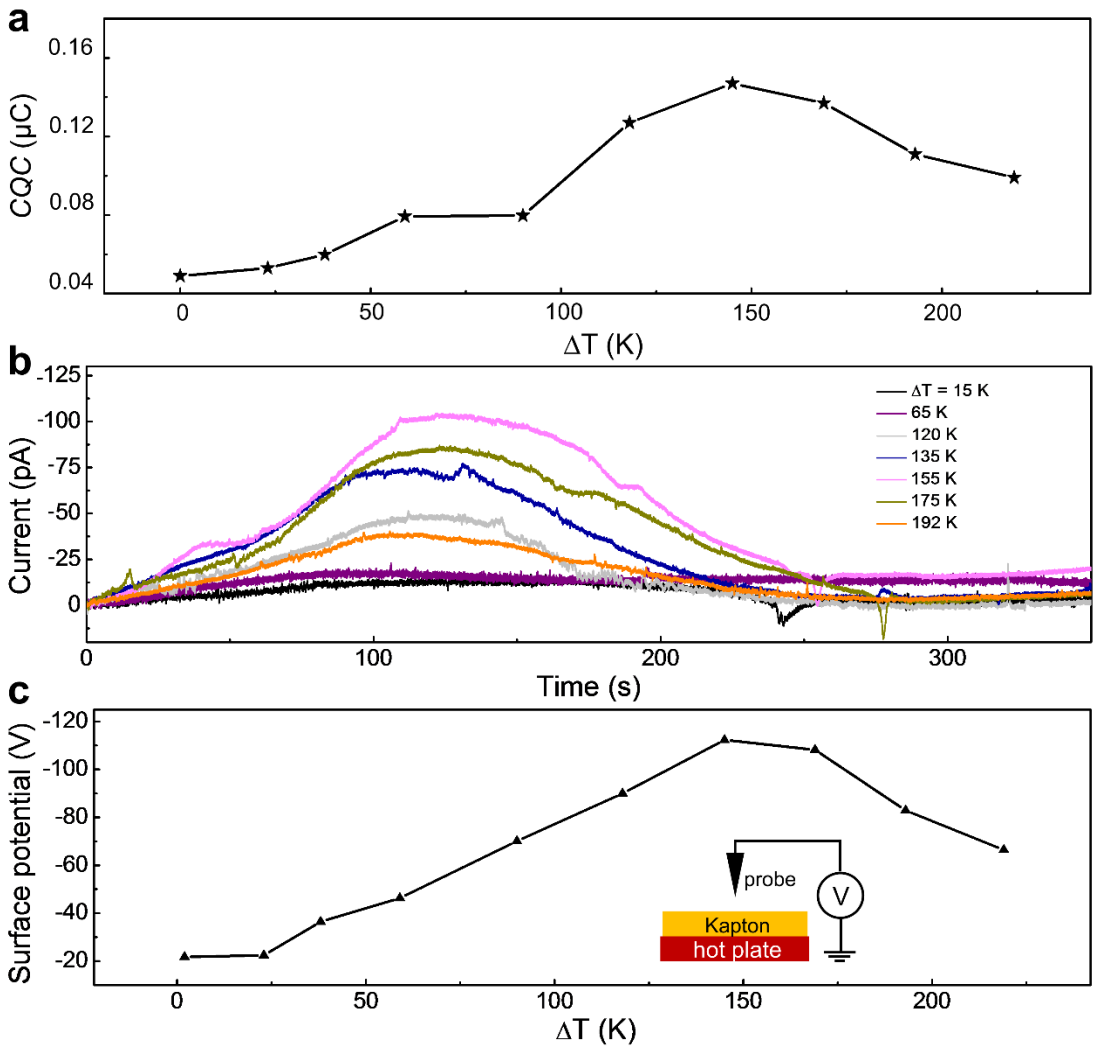

Figure 3. Characterization of the effect of ΔT on TDNG. (**a**) The relationship between transferred short-circuit current charges of TDNG and ΔT. (**b**) The thermally stimulated discharge current and (**c**) the surface potential of Kapton after friction at different ΔT.

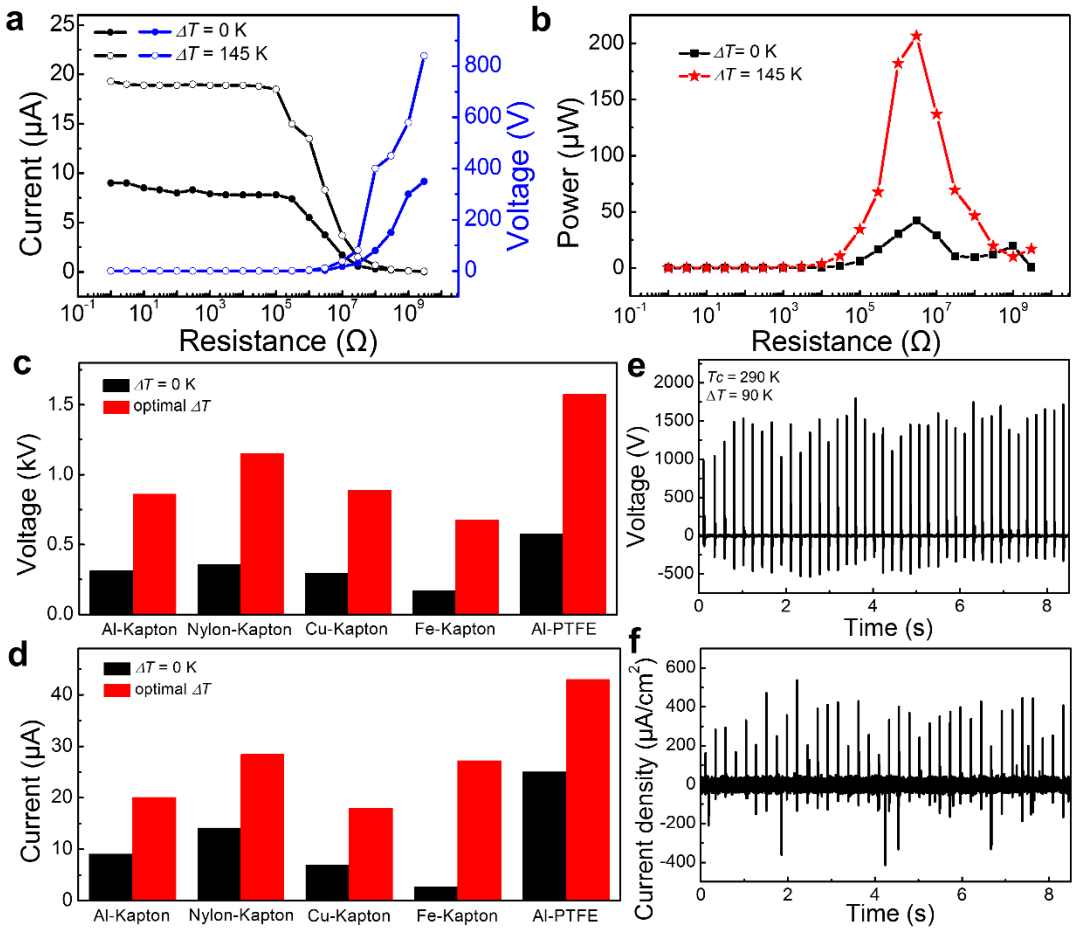

Figure 4. The influence of ΔT on TDNG with different friction materials. (**a**) The output voltage, current and (**b**) output power of TDNG with different external circuit load resistance when ΔT is equal to 0 K and 145 K, respectively. (**c**) The open-circuit voltage and (**d**) short-circuit current with different friction materials when ΔT=0 K and optimal ΔT. (**e**) The open-circuit voltage (~1500 V) and (**f**) short-circuit current density (~ 396 μA/cm^2) of Al-PTFE TENG at ΔT=90 K.

Materials	Al-Kapton	PA6-Kapton	Cu-Kapton	Fe-Kapton	Al-PTFE
Optimum ΔT	145 K	144 K	145 K	143 K	90 K
V_O/V_R	2.7	3.2	3.0	3.9	2.7
I_O/I_R	2.2	2.0	2.6	10	1.69

Table 1. The ratio between open-circuit voltage and short-circuit current of different materials based TDNG under optimal ΔT and ΔT = 0 K.

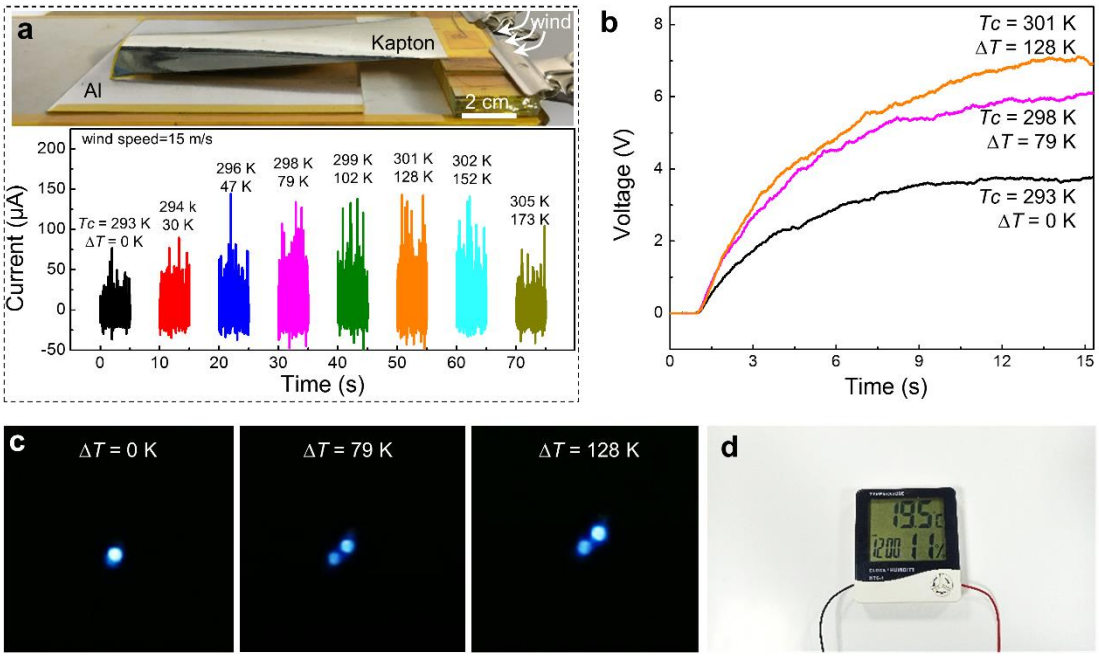

Figure 5. Demonstration of the wind-driven TDNG working on the surface of high temperature object. (**a**) Top part is the photograph of wind-driven TDNG on a hot plate. Bottom part is the short-circuit current of the wind-driven TDNG under different ΔT (wind speed: 15 m/s). (**b**) Charging curves of a capacitor with 1 μF capacitance by wind-driven TDNG under different ΔT (0 K, 79 K, 128 K). (**c**) LEDs are used for temperature indicator. (**d**) Photograph of a temperature-humidity sensor powered by wind-driven TDNG.

Figures

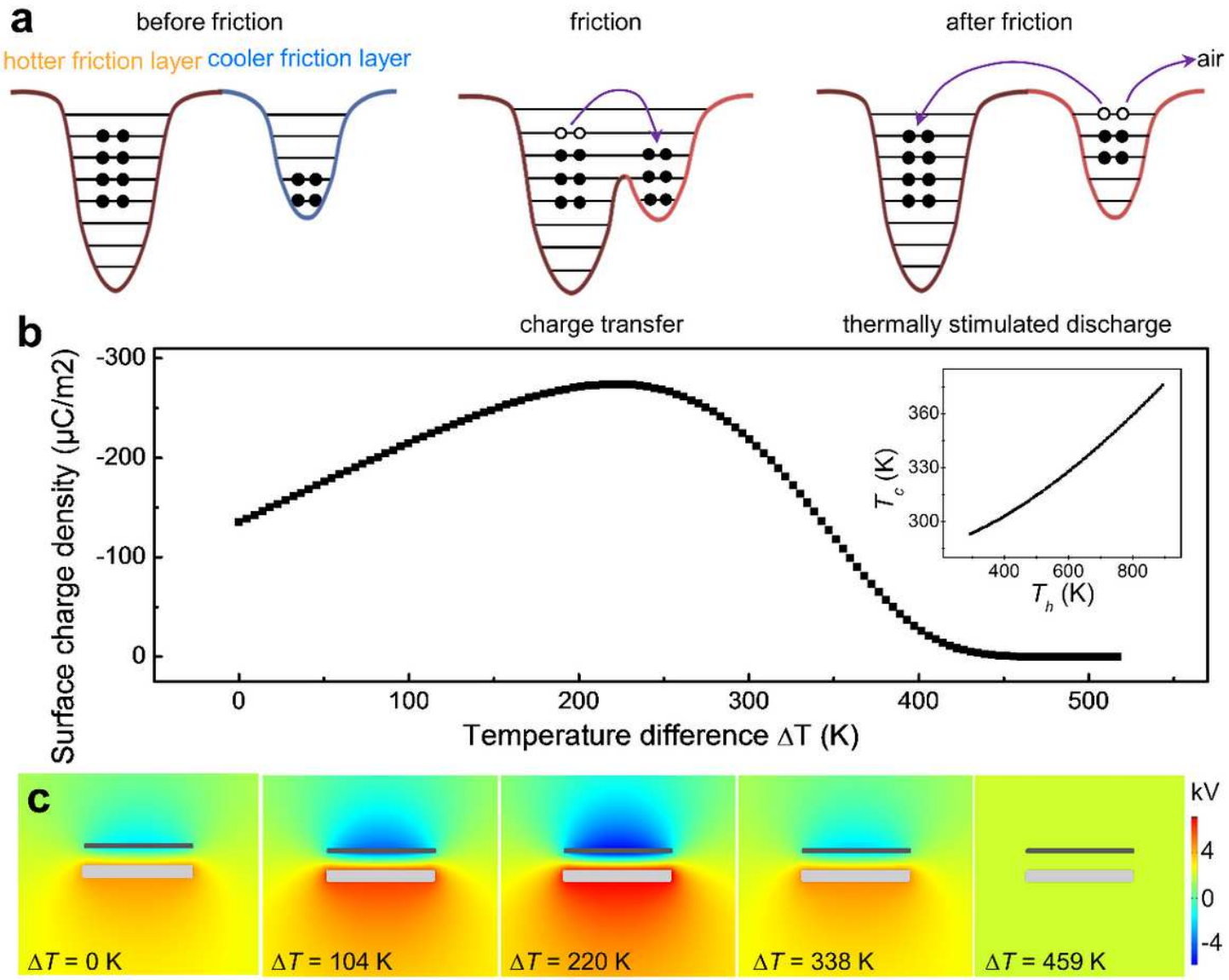

Figure 1

The influence of temperature difference between different friction layers on TENG's performance. (a) Effect of ΔT on charge transfer and dissipation. (b) Numerical simulations of the relationship between ΔT and the short-circuit transfer charge density. The right upper is the relationship between the temperature of the hotter part and the cooler part. (c) The potential distribution of TENG under different ΔT.

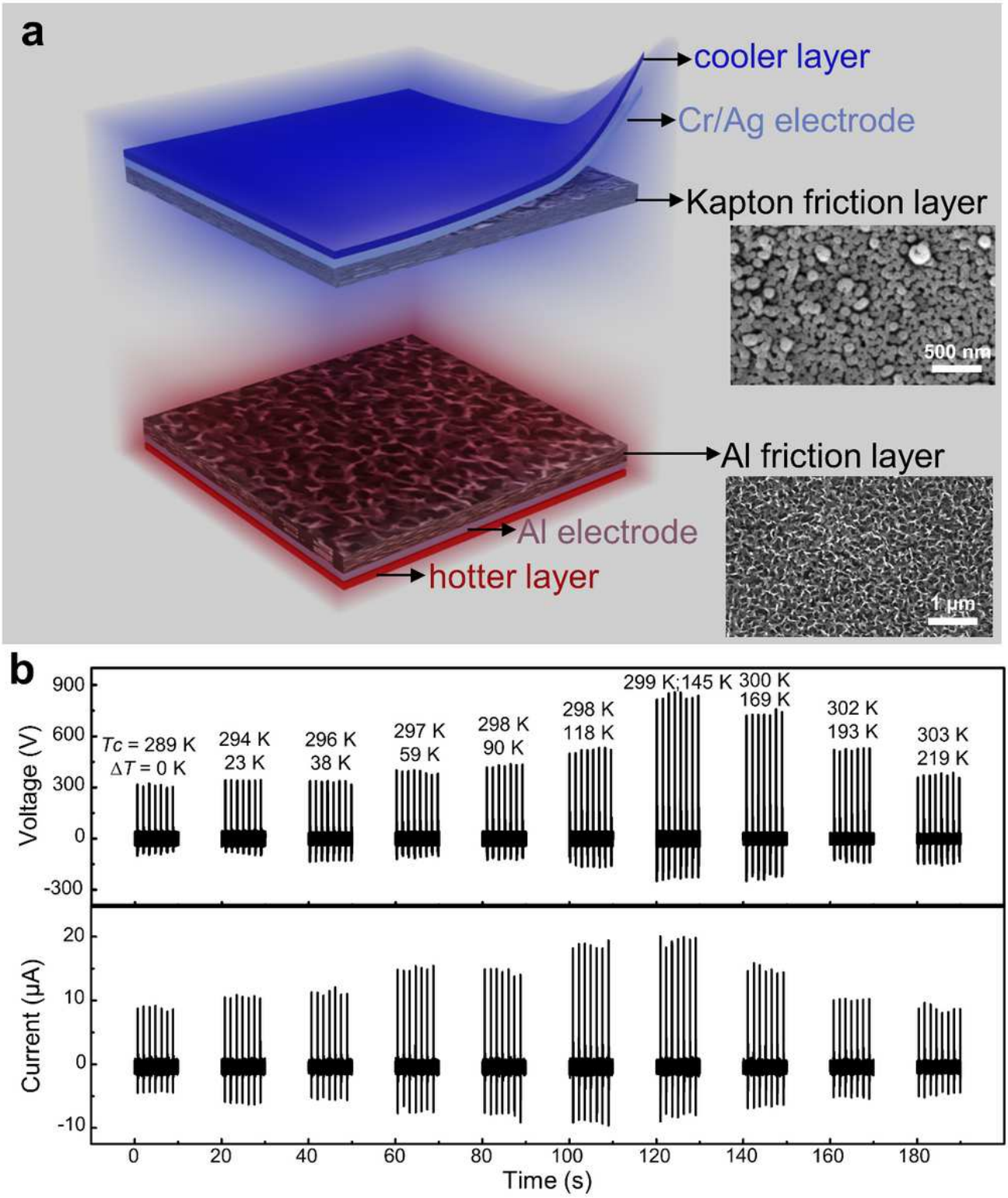

Figure 2

Design and output performance of TDNG. (a) Schematic diagram of TDNG. Insert are SEM images of nanostructures on Kapton and Al. (b) The open-circuit voltage and short-circuit current of TDNG under different ΔT.

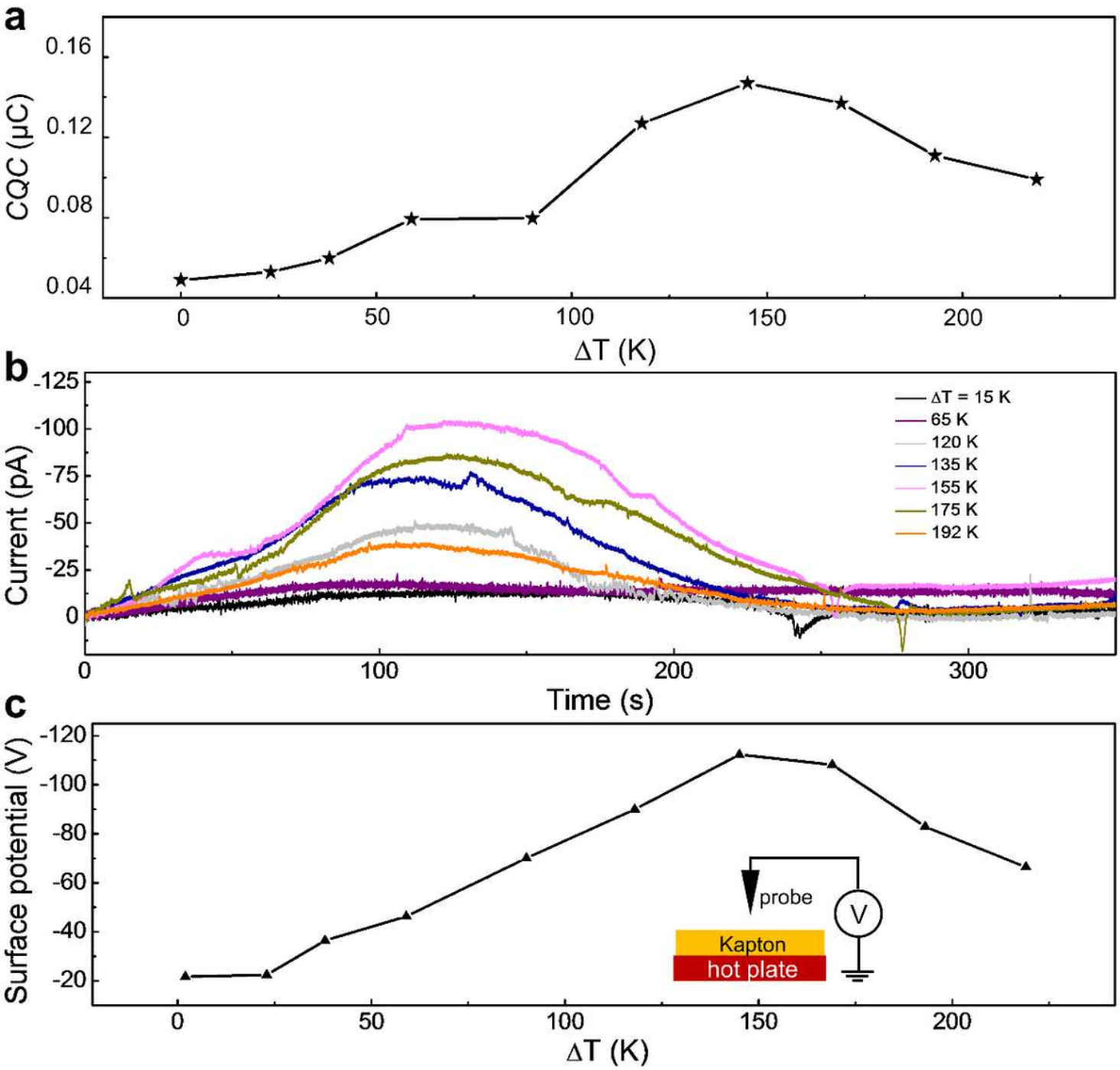

Figure 3

Characterization of the effect of ΔT on TDNG. (a) The relationship between transferred short-circuit current charges of TDNG and ΔT. (b) The thermally stimulated discharge current and (c) the surface potential of Kapton after friction at different ΔT.

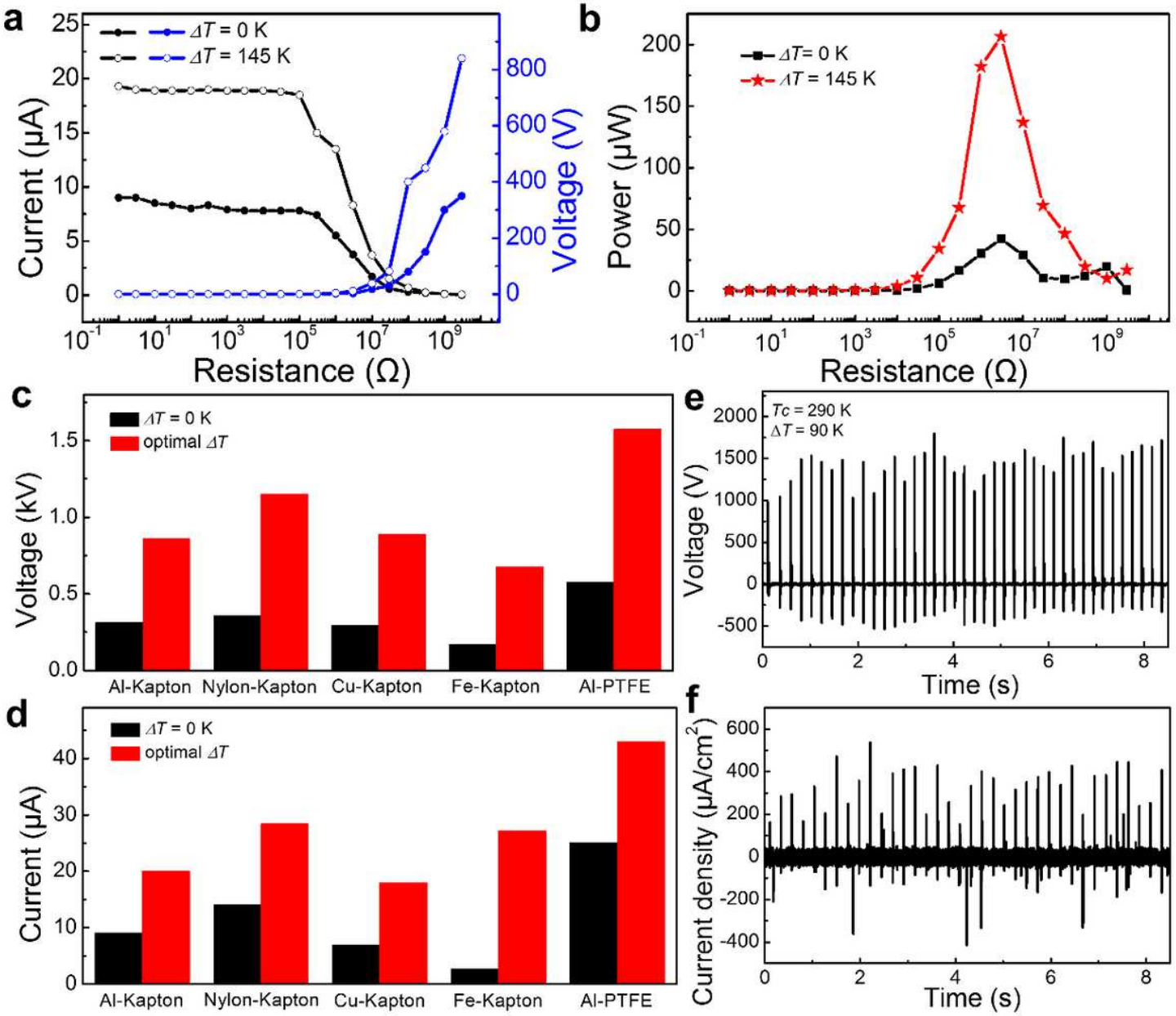

Figure 4

The influence of ΔT on TDNG with different friction materials. (a) The output voltage, current and (b) output power of TDNG with different external circuit load resistance when ΔT is equal to 0 K and 145 K, respectively. (c) The open-circuit voltage and (d) short-circuit current with different friction materials when ΔT=0 K and optimal ΔT. (e) The open-circuit voltage (~1500 V) and (f) short-circuit current density (~ 396 μA/cm2) of Al-PTFE TENG at ΔT=90 K.

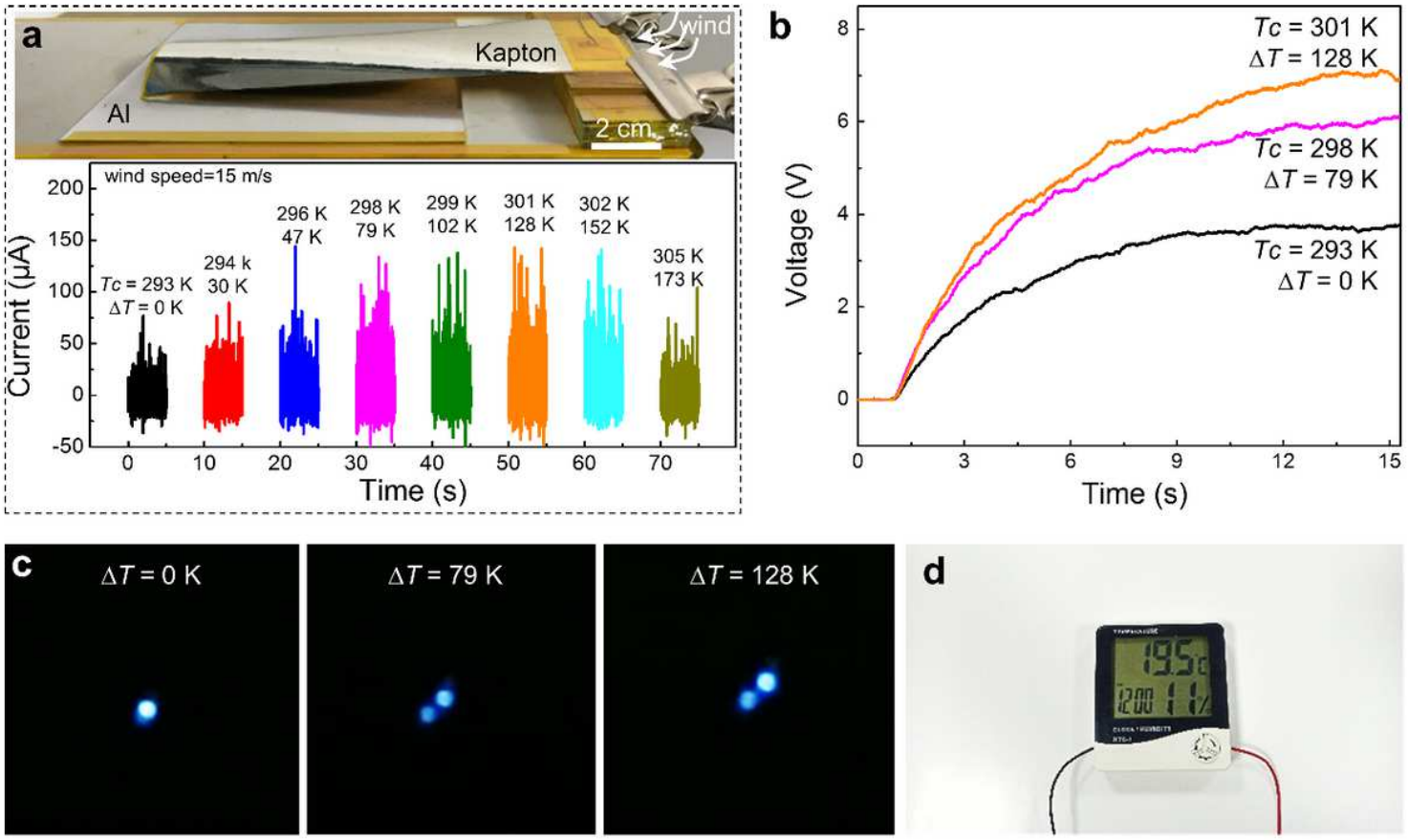

Figure 5

Demonstration of the wind-driven TDNG working on the surface of high temperature object. (a) Top part is the photograph of wind-driven TDNG on a hot plate. Bottom part is the short-circuit current of the wind-driven TDNG under different ΔT (wind speed: 15 m/s). (b) Charging curves of a capacitor with 1 μF capacitance by wind-driven TDNG under different ΔT (0 K, 79 K, 128 K). (c) LEDs are used for temperature indicator. (d) Photograph of a temperature-humidity sensor powered by wind-driven TDNG.

Supplementary Files

This is a list of supplementary files associated with this preprint. Click to download.

- SupplementaryInformation.docx